Role of input angular momentum and target deformation on the incomplete-fusion dynamics in the $^{16}O + ^{154}Sm$ system at $E_{Lab} = 6.1$ MeV/nucleon

D. Singh,[1,*] Sneha B. Linda,[1] Pankaj K. Giri,[1] Amritraj Mahato,[1] R. Tripathi,[2] Harish Kumar,[3] M. Afzal Ansari,[3] N. P. M. Sathik,[4] Rahbar Ali,[5] R. Kumar,[6] S. Muralithar,[6] and R. P. Singh[6]

[1]*Centre for Applied Physics, Central University of Jharkhand, Ranchi-835 205, India*
[2]*Radio-chemistry Division, Bhabha Atomic Research Centre, Mumbai-400 085, India*
[3]*Department of Physics, Aligarh Muslim University, Aligarh-202 002, India*
[4]*Department of Physics, Jamal Mohammed College, Trichurapalli-620 020, India*
[5]*Department of Physics, G.F.(P.G.), College, Shahjahanpur-242 001, India*
[6]*Inter-University Accelerator Centre, Aruna Asaf Ali Marg, New Delhi-110 067, India*

(Received 21 September 2017; revised manuscript received 5 January 2018; published 7 June 2018)

Spin distributions of nine evaporation residues ^{164}Yb(xn), ^{163}Tm(pxn), ^{168,167}Er($2pxn$), $^{163-161}$Ho(αpxn), ^{164}Dy($\alpha 2pxn$), and ^{160}Dy($2\alpha xn$) produced through complete- and incomplete-fusion reactions have been measured in the system $^{16}O + ^{154}Sm$ at projectile energy = 6.1 MeV/nucleon using the in-beam charged-particle ($Z = 1,2$)–γ-ray coincidence technique. The results indicate the occurrence of incomplete fusion involving the breakup of ^{16}O into ^{4}He + ^{12}C and/or ^{8}Be + ^{8}Be followed by fusion of one of the fragments with target nucleus ^{154}Sm. The pattern of measured spin distributions of the evaporation residues produced through complete and incomplete fusion are found to be entirely different from each other. It has been observed from these present results that the mean input angular momentum for the evaporation residues produced through complete fusion is relatively lower than that of evaporation residues produced through incomplete-fusion reactions. The pattern of feeding intensity of evaporation residues populated through complete- and incomplete-fusion reactions has also been studied. The evaporation residues populated through complete-fusion channels are strongly fed over a broad spin range and widely populated, while evaporation residues populated through incomplete-fusion reactions are found to have narrow range feeding only for high spin states. Comparison of present results with earlier data suggests that the value of mean input angular momentum is relatively higher for a deformed target and more mass asymmetric system than that of a spherical target and less mass asymmetric system by using the same projectile and the same energy. Thus, present results indicate that the incomplete-fusion reactions not only depend on the mass asymmetry of the system, but also depend on the deformation of the target.

DOI: 10.1103/PhysRevC.97.064604

I. INTRODUCTION

The study of heavy ion (HI) induced reactions, particularly complete-fusion (CF) and incomplete-fusion (ICF) dynamics at projectile energy just above the Coulomb barrier [1–9], has been an important area from the past few decades. Several reaction channels may open in the interaction of two heavy ions and a transfer of cluster of nucleons may take place. Britt and Quinton [10] were the first to observe the production of "fast α particles" in the breakup of projectiles ^{12}C, ^{14}N, and ^{16}O into α clusters in an interaction with the surface of the target nucleus at bombarding energies ≈10.5 MeV/A. Subsequently, Galin *et al.* [11] also observed the breakup of projectiles and called such reactions, leading to the emission of "fast" α particles, "ICF reactions" or "breakup fusion reactions." However, major advances in the study of ICF dynamics has taken place after the measurement of charged-particle–γ-ray coincidence by Inamura *et al.* [12] for the $^{14}N + ^{159}Tb$ system at beam energy ≈7 MeV/nucleon. The studies by Parker *et al.* [13], Tomar *et al.* [14,15], Sharma *et al.* [16], and Singh *et al.* [17] showed the onset of the ICF process just above the Coulomb barrier at bombarding energies around 5–7 MeV/nucleon. Morgenstern *et al.* [18] showed that ICF reactions significantly contribute to the total reaction cross section for mass asymmetric systems at the same relative velocity, and hence observed the effect of entrance channel mass asymmetry on ICF fraction. Earlier studies carried out on a large number of projectile target combinations have brought out the entrance channel mass asymmetry dependence of ICF reaction, with ICF probability being higher in a mass asymmetric system than in a mass symmetric system [19–22]. Gavron *et al.* [23], Westerberg *et al.* [24], and Geoffroy *et al.* [25] reported the studies based on light ions in coincidence with prompt γ rays of evaporation residues. Siwek-Wilczynska *et al.* [26] provided a classical picture to understand the ICF dynamics. Yamada *et al.* [27] and Zolonwski *et al.* [28] pointed out that the projectile like fragments (PLFs) are emitted during the interaction of a projectile with a target based on charged-particle ($Z = 1,2$) coincidence with prompt γ rays. Semiclassical theory of HI interaction categorizes the CF and ICF processes on the basis of driving input angular momentum ℓ imparted in the system.

*dsinghcuj@gmail.com

According to the sharp cutoff approximation [29–31] the ICF process lies in the range $\ell_{crit} \leqslant \ell \leqslant \ell_{max}$,while the CF process lies in the driving input angular momentum range $0 \leqslant \ell \leqslant \ell_{crit}$. It may be understood in the following way: for CF, the attractive nuclear potential overcomes the repulsive Coulomb and centrifugal potentials in central and near central collisions. Consequently, at a small value of impact parameter and relatively lower projectile energy the entire projectile fuses with the target nucleus leading to the formation of a fully equilibrated compound nucleus (CN). On the other hand, at relatively larger values of impact parameter and higher projectile energies, an incompletely fused composite (IFC) system comprised of a part of the projectile plus the target appears in the exit channel, wherein the involvement of driving input angular momentum ℓ is relatively larger than that needed for the CF process to take place. At this stage if the driving input angular momentum exceeds the critical limit (ℓ_{crit}) for CF, no fusion can occur unless a part of the projectile is emitted to reduce the driving input angular momentum. Several investigators [32,33] pointed out that after emission of a part of the projectile during the ICF dynamics, the remaining part of the projectile has resulting input angular momentum less than or equal to its own critical limit for fusion to occur. Eventually, an IFC system is formed via partial fusion of the projectile. In this case the IFC system has relatively less mass and charge than that of an excited compound nucleus formed in the CF process. It is therefore assumed that the evaporation residues produced through the ICF process are associated with ℓ values above the ℓ_{crit} for CF. Moreover, Gerschel [34] suggested that the localization of the ℓ window depends on the target deformation at energies below 10 MeV/nucleon. In the case of deformed target nuclei peripheral collisions are observed with ℓ values in the vicinity of ℓ_{crit} for CF, while for spherical target nuclei, the ℓ window is found to be centered around the ℓ values $\leqslant 0.5\ \ell_{crit}$. Both CF and ICF processes contribute significantly below and above their input angular momentum limits and there is no sharp cutoff limit of input angular momentum [35].

Various dynamical models have been proposed to explain the features of ICF apart from experimental studies, viz., the breakup fusion (BUF) model of Udgawa and Tamura [36] qualitatively explained the kinetic energy spectra and angular distributions of ejectiles. The sum-rule model of Wilczynski *et al.* [37] predicts that ICF mainly occurs in the peripheral interactions and are localized in angular momentum space above the critical angular momentum for complete fusion (CF). On the other hand, Mermaz *et al.* [38] explained the energy and angular distribution of the projectilelike fragments (PLFs) using a modified distorted-wave Born approximation (DWBA) formalism for surface transfer reactions. Other theoretical models are the promptly emitted particles (PEPs) model [39], the hot spot model [40], and the Fermi-jet model [41], etc. As a matter of fact all these models have been used to fit the experimental data of PLFs at projectile energy above 10 MeV/nucleon and none of the above proposed models is able to fit the experimental data at bombarding energy below 7 MeV/A. Hence, study of ICF dynamics is still an active area of investigation. Dracoulis *et al.* [42] suggested that ICF can be used as a tool for population of high spin states in the final reaction products even at low bombarding energies. Recent studies based on HI using the particle-γ coincidence technique suggest significant change in the spin distributions and feeding intensity profiles of evaporation residues (ERs) [43–47]. Keeping in view the above aspects, an attempt has been made to understand the ICF dynamics by the particle-γ coincidence technique.

In the present work investigation of driving input angular momenta in CF and ICF, the role of target deformation on ICF, the amount of mass transfer and entrance channel mass-asymmetry effect on ICF dynamics by measuring the spin distributions of ERs using the particle-γ coincidence technique has been done. Major findings of the present studies have been summarized in Ref. [48]. Here we present the detailed results. Some correlation between the driving angular momenta of CF and ICF channels has been drawn to investigate the above mentioned effects. This paper is organized in the following parts. The experimental details and analysis of spin distribution data are given in Secs. II and III. Interpretation of spin distribution and pattern of feeding intensity of CF and ICF and comparison with earlier data [45] are discussed in Secs. IV and V. The summary and conclusions of the present study are given in the last section of this paper.

II. EXPERIMENTAL TECHNIQUE DETAILS

The present charged-particle ($Z = 1,2$)–γ-ray coincidence experiments have been carried out using Gamma Detector Array (GDA) coupled with Charged Particle Detector Array (CPDA) at the 15UD Pelletron Accelerator facility of the Inter University Accelerator Centre (IUAC), New Delhi, India. The self-supporting target of ^{154}Sm (enrichment $\approx$98.69%) of thickness $\approx$3.1 mg/cm^2 was pasted on annular Al-target holders having a concentric hole of 1.0 cm diameter. The weighing as well as particle transmission method using ^{241}Am were adopted for the thickness determination of the target. Gamma Detector Array (GDA) consists of 12 Compton suppressed n-type high purity germanium (HPGe) detectors at angles 45°,99°,153° with respect to the beam direction, with the arrangement of four detectors at each of these angles. All 12 HPGe detectors are fixed at a distance of 18 cm from the target position in the array and the CPDA, a group of 14 Phoswich detectors, are housed in a small scattering chamber of 14 cm diameter. In the CPDA scattering chamber, seven charged-particle detectors (CPDs) were placed on the top and seven in the bottom of the chamber. These 14 CPDs were arranged in two truncated hexagonal pyramids. The bases of the all pyramids are in the horizontal plane with each other having trapezoidal shape. The two hexagonal detectors are inserted from the top and bottom. The total solid angle coverage is greater than 90% of 4π taking into account the opening for beam entrance and exit. The corners of the trapezoids are cut off for the entrance and exit of the beam and for target support purpose. All 14 detectors of CPDA are divided into three angular zones. There are four CPDA detectors at "forward angles (F)" (10°–60°), four detectors at "backward angles (B)" (120°–170°), and six detectors "sideways (S)," i.e., between 60° and 120°. Each CPD consists of the following components: (i) a Phoswich detector made of plastic scintillator, (ii) an optical guide, and (iii) a photomultiplier tube (PMT). A

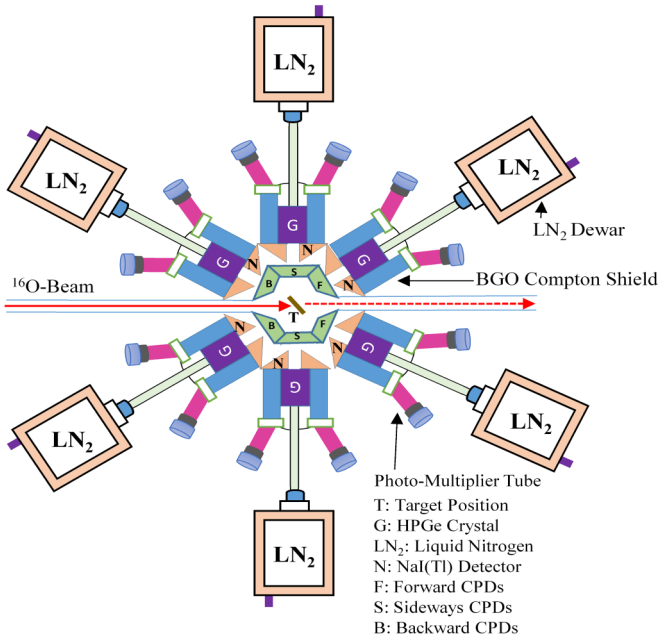

FIG. 1. A schematic diagram of experimental setup of Gamma Detector Array coupled with Charged Particle Detector Array (CPDA) used for the particle–γ-ray coincidence experiment for $^{16}O + ^{154}Sm$ system at projectile energy of 97.5 MeV.

Phoswich detector is made by combining two dissimilar plastic scintillators optically coupled to a PMT. One of the detectors (thin-BC400-0.1 mm) has a fast rise time giving information on the type (Z) of the particle detected, based on the energy (ΔE) deposited by the particle. The second detector (thick-BC444-5 mm) has a slow decay constant containing total energy (E) deposited by the traversing particle(s). The light collection is done by properly shaped Ultraviolet Transmitting (UVT) light guides coupled to 25 mm diameter miniature phototubes. Particle (α and proton) identification has been done based on pulse height analysis from fast-slow plastic Phoswich detectors. A schematic diagram of the experimental setup of the Gamma Detector Array coupled with Charged Particle Detector Array (CPDA) used for the particle-γ coincidence experiment for the $^{16}O + ^{154}Sm$ system at a projectile energy of 97.5 MeV is shown in Fig. 1. The distance from the target to each CPD was 7 cm. The target was mounted at 45° with respect to the beam direction inside the CPDA chamber at the center on a stainless steel target ladder. In order to minimize the background γ rays coming from the target holder material, the target holder was covered with tantalum foil of the same size as that of target holder. A tantalum collimator of 6 mm diameter was used inside the scattering chamber to collimate the beam in the center of the target. The target was bombarded with $^{16}O^{+7}$ beam of energy 100 MeV with the beam current ~3 pnA, which was stopped completely in a thick tantalum sheet attached with Faraday cup at end of the beam line at a distance of about five meters. The beam energy at the center of the target was 97.5 MeV due to beam energy degradation. The energy loss of the beam in the target was calculated using the code SRIM [49]. In this experiment two current integrators were used to read the current on collimator and

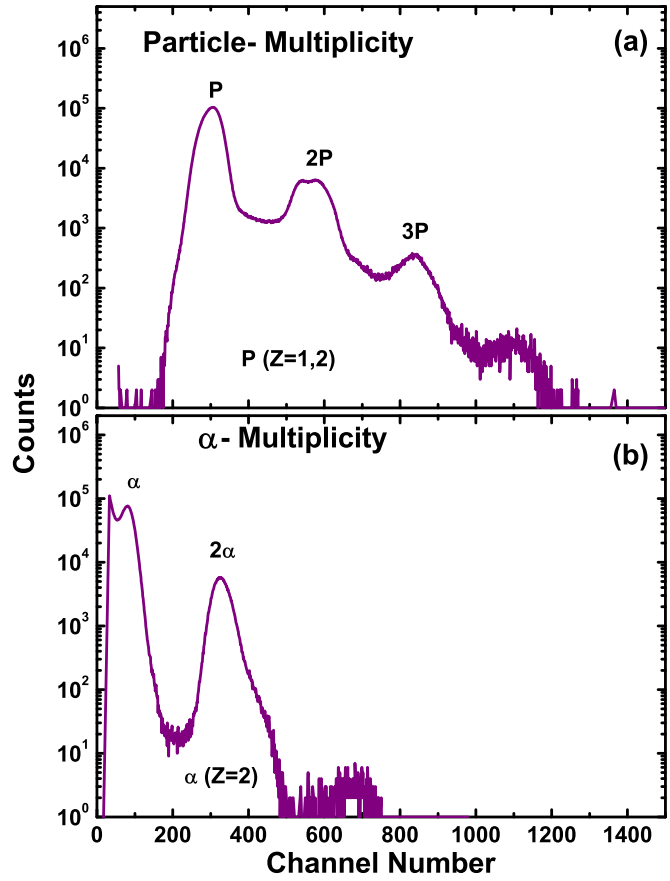

FIG. 2. Multiplicity spectra recorded for (a) charged particles ($Z = 1,2$) and (b) α particles for the $^{16}O + ^{154}Sm$ system at projectile energy of 97.5 MeV.

Faraday cup for beam focusing purpose on the target. The tantalum collimator was at a distance of 4.5 cm before the target position. One current integrator was connected with the collimator and another connected with a Faraday cup. The current was minimized on the collimator and maximized on the Faraday cup for the proper alignment. A LINUX-based computer system was used for data acquisition. The on-line multiparameter data were recorded by the data acquisition software CANDLE [50] in event-by-event LIST mode and stored in the computer hard disk. The timing information from all detectors was recorded using the time-to-digital converter (TDC) module. The identification of charged particles (proton and α) has been done through Phoswich detectors (inbuilt $\Delta E - E$ structure), which was based on pulse height analysis. The multiplicity spectra for charged particles ($Z = 1,2$) and α particles were recorded to define the charged particle-γ coincidence and are shown in Figs. 2(a) and 2(b) respectively. Detailed information on construction and working of CPDA are given in [51]. In the present experiment two groups of α particles were expected to be detected by forward angle (F) CPDs: (i) the fusion-evaporation (CF) α particles of average energy $E_{\alpha\text{-CF}} \approx 20$ MeV and (ii) the ICF "fast" α particles of energy $E_{\alpha\text{-ICF}} \approx 25$ MeV. The α particles emitted during the breakup of the ^{16}O-ion beam move in the forward cone. The energy and velocity of these α particles are larger than those of α particles

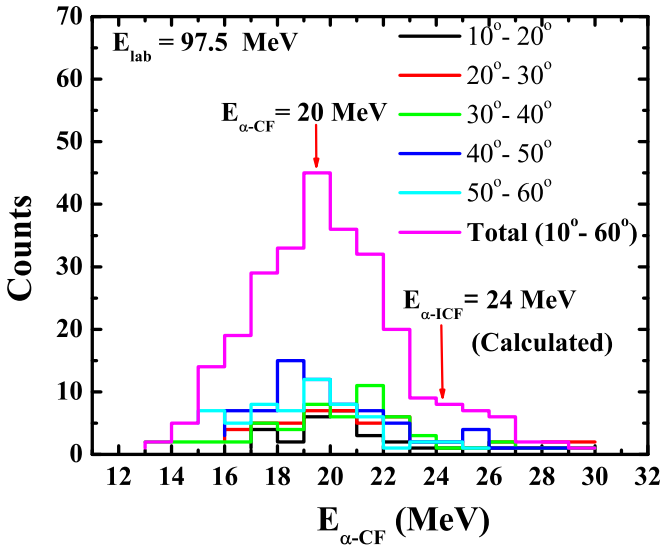

FIG. 3. Fusion-evaporation α-particle energy profile in forward cone predicted by PACE4 for the system ^{16}O + ^{154}Sm at projectile energy of 97.5 MeV.

emitted from the compound nucleus. These α particles are called "fast" α particles. The fusion-evaporation α-particle energy profile in the forward cone predicted by PACE4 [23] for the system ^{16}O + ^{154}Sm at a projectile energy of 97.5 MeV is shown in Fig. 3. To detect only fast α particles in the forward cone, in front of each of the four forward cone CPDs, aluminum absorbers of appropriate thickness were used to stop low energy "evaporation"α particles ($E_{\alpha\text{-CF}} \approx 20$ MeV). All HPGe detectors in the GDA setup were precalibrated by using standard γ sources ^{60}Co, ^{133}Ba, and ^{152}Eu of known strength. A ^{241}Am-source was used to calibrate the CPDA. Coincidences were taken between charged particles ($Z = 1,2$) and the prompt γ rays emitted from the evaporation residues formed during the interaction of ^{16}O with ^{154}Sm. γ-ray spectra in coincidence with charged particles ($Z = 1,2$) detected forward, backward, and sideways by Phoswich detectors were recorded. Various factors contributing to the uncertainties in the present measurements and their estimates are as follows: (i) the nonuniformity of the target foil may introduce an error $<3\%$; (ii) $<5\%$ uncertainty due to the fluctuations in the beam current during the irradiation; (iii) uncertainty in the efficiency of high purity germanium (HPGe) detectors was minimized due to recording the efficiency spectra for a much longer period; (iv) the error in the γ-ray peak fitting has been determined by employing the peak fitting software CANDLE [50]. The overall total uncertainty in the experimentally measured relative yields of evaporation residues is estimated to be $\leqslant 15\%$.

III. ANALYSIS OF SPIN DISTRIBUTIONS

The off-line data analysis has been done by using the software CANDLE [50]. Four coincidence gating conditions particle–backward gated, particle-forward gated, α-backward gated, and α–forward gated have been applied on all the observed γ-ray spectra. To improve the statistics in experimental data, all gated spectra from different runs for a particular gating condition have been summed up. Identification of specific CF and ICF reaction channels were done using singles spectra and/or different gated spectra. Spin distributions for different evaporation residues have been extracted by measuring the relative production yields of different levels in the rotational bands. The prompt-γ energies and their spin states used in the present work have been taken from RADWARE level scheme directory [52]. Several evaporation residues populated through xn channels (CF reaction channels) have been identified from singles spectra. In order to obtain proton-gated spectra for the identification of pxn and $2pxn$ channels, the α-backward gated spectrum has been subtracted from the particle-backward gated spectrum. The αpxn, $\alpha 2pxn$, and $2\alpha xn$ channels (fast α particle emitted from projectile breakup) populated through the ICF reaction have been identified from particle-forward gated and α-forward gated spectra. The CF and ICF reaction channels can also be identified by comparing the spectra gated with forward and backward going α particles. ICF would thus lead to a "harder" α spectrum in the forward direction than that expected for α evaporation from a compound nucleus. γ-ray energy spectra observed in interaction of the ^{16}O-ion beam with a ^{154}Sm target at 97.5 MeV are shown in Fig. 4. Spin distributions of various ERs produced through CF and ICF reaction channels and the relative production yields corresponding to the levels of prompt-γ transitions have been determined using the methodology adopted by Inamura *et al.* [12], Singh *et al.* [43–45], and Sharma *et al.* [46,47]. Measured relative production yields have been normalized with respect to the highest experimentally measured values ($^{\text{Maxm}}_{\text{Obsd}}Y$) at lowest observed spin ($^{\text{Minm}}_{\text{Obsd}}J$) for the respective channels for better comparison of different CF and ICF channels. The normalized production yields have been plotted as a function of experimentally observed spin ($^{\text{Expl}}_{\text{Obsd}}J$) corresponding to prompt-γ transitions of identified evaporation residues. The measured spin distributions for different evaporation residues mentioned above produced through CF and ICF reaction channels have been fitted by a function of the type given below [29]:

$$Y = Y_0/[1 + \exp(_{\text{Obsd}}J - {}_{\text{Mean}}J)/\Delta], \tag{3.1}$$

where Δ is related to the width of mean input angular momentum $_{\text{Mean}}J$, and Y_0 is the normalization constant. Here, $_{\text{Mean}}J$ is a sensitive parameter, which provides the qualitative information about the driving input angular momentum ℓ associated with various CF and ICF reaction channels. The measured spin distribution produced in CF (fusion evaporation) and ICF reaction channels are displayed in Figs. 5(a) and 5(b). The spin distributions are the normalized yield profiles as a function of observed spin ($_{\text{Obsd}}J$) of evaporation residues. The solid arrow headed lines correspond to the spin at which the normalized yield falls to be half for the ERs produced through CF and ICF reaction. The spins at which the normalized yield is half is defined as mean input angular momentum. The CF and ICF reaction channels can also be identified by comparing the spectra of forward and backward going α particles.

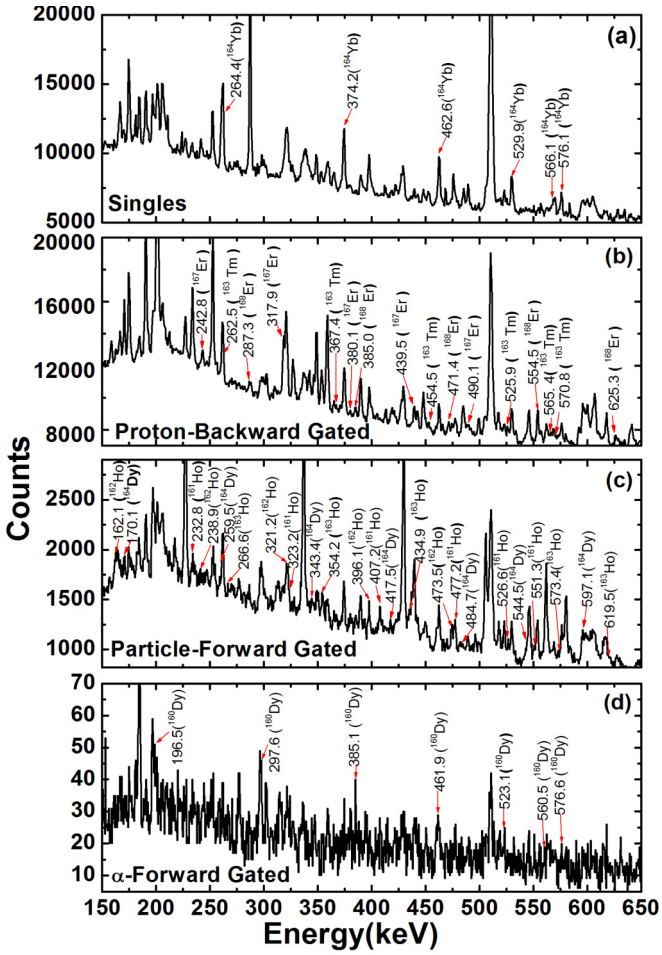

FIG. 4. γ-ray energy spectra with different gating conditions (a) singles, (b) proton–backward gated, (c) particle–forward gated, and (d) α–forward gated, observed for the $^{16}O + ^{154}Sm$ system at projectile energy of 97.5 MeV.

IV. INTERPRETATION OF SPIN DISTRIBUTIONS AND PATTERN OF FEEDING INTENSITY IN CF AND ICF DYNAMICS

The measured spin distributions of nine ERs, namely, $^{164}Yb(xn)$, $^{163}Tm(pxn)$, $^{168,167}Er(2pxn)$, $^{163-161}Ho(\alpha pxn)$, $^{164}Dy(\alpha 2pxn)$, and $^{160}Dy(2\alpha xn)$ populated through CF and/or ICF reaction channels respectively are plotted in Figs. 5(a) and 5(b). The measured spin distributions of the four ERs $^{164}Yb(xn)$, $^{163}Tm(pxn)$, and $^{168,167}Er(2pxn)$ are identified from singles and proton-backward gated spectra. These ERs, ^{164}Yb, ^{163}Tm and $^{168,167}Er$, are populated through CF via the following different reaction routes:

(i) $^{16}O + ^{154}Sm \rightarrow ^{170}Yb^* \rightarrow ^{164}Yb + xn \quad (x = 6)$,
(ii) $^{16}O + ^{154}Sm \rightarrow ^{170}Yb^* \rightarrow ^{163}Tm + pxn \quad (x = 6)$,
(iii) $^{16}O + ^{154}Sm \rightarrow ^{170}Yb^* \rightarrow ^{168}Er + 2pxn \quad (x = 0)$,
(iv) $^{16}O + ^{154}Sm \rightarrow ^{170}Yb^* \rightarrow ^{167}Er + 2pxn \quad (x = 1)$.

The reaction channels indicate the occurrence of complete fusion of ^{16}O with target nucleus ^{154}Sm. The measured spin

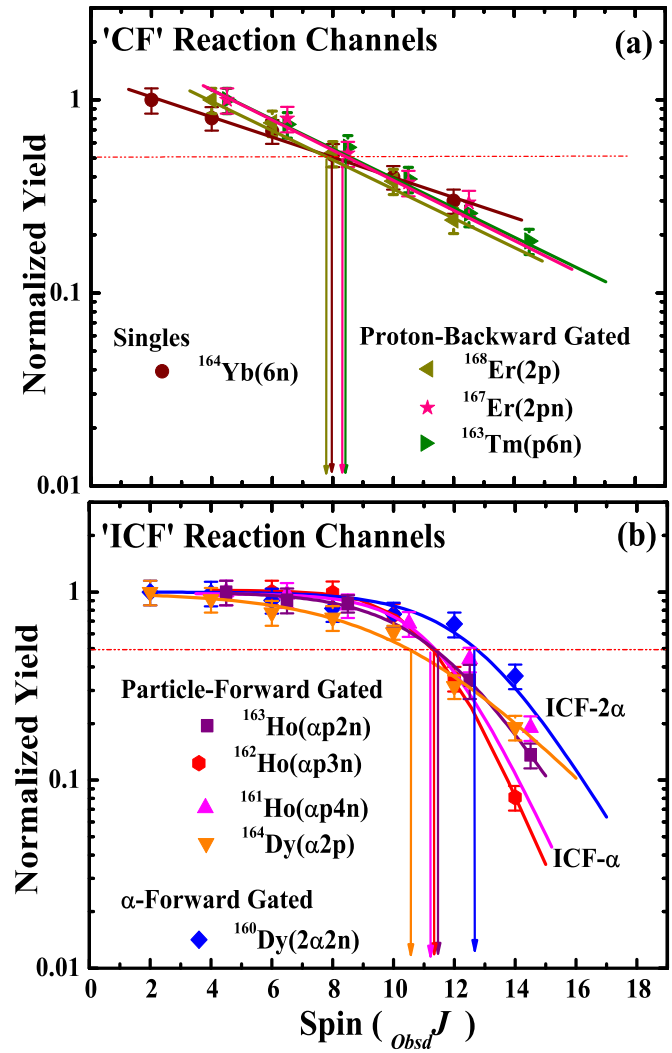

FIG. 5. Measured spin distributions for the evaporation residues (a) ^{164}Yb, ^{163}Tm, and $^{168,167}Er$ populated through CF reactions and (b) $^{163,162,161}Ho$ and $^{164,160}Dy$ populated through ICF reactions in interaction of ^{16}O with ^{154}Sm at 97.5 MeV. The straight lines are the least square fit and curves passing through experimental data points are the best fits using the method given in the text.

distributions of the four ERs, ^{164}Yb, ^{163}Tm, and $^{168,167}Er$, populated through CF reaction channels are plotted in Fig. 5(a). It can be seen from this figure that the spin distributions show a sharp exponential fall in intensities towards the high spin states. It gives an indication of strong feeding during the deexcitation of CN towards the lowest member of the yrast line transitions. However, the spin ($_{Mean}J$) at half yield, i.e., the mean input angular momentum, is found to be $\approx 8\hbar$ for the ERs produced through xn, pxn, and $2pxn$ emitting channels (associated with CF).

The ERs $^{163-161}Ho(\alpha pxn)$, $^{164}Dy(\alpha 2pxn)$, and $^{160}Dy(2\alpha xn)$ respectively populated through ICF have been identified by particle-forward gated and α-forward gated spectra recorded in the forward cone ($10^\circ - 60^\circ$). These ERs, $^{163-161}Ho(\alpha pxn)$, $^{164}Dy(\alpha 2pxn)$, and $^{160}Dy(2\alpha xn)$, are populated through ICF via the following different reaction routes:

(i) $^{16}O(^{12}C+\alpha)+{}^{154}Sm \rightarrow {}^{12}C+{}^{154}Sm$
$\rightarrow {}^{166}Er^{*}+\alpha$ (spectator)
$\rightarrow {}^{163}Ho+\alpha$ (spectator) $+ pxn \quad (x=2)$,
(ii) $^{16}O(^{12}C+\alpha)+{}^{154}Sm \rightarrow {}^{12}C+{}^{154}Sm$
$\rightarrow {}^{166}Er^{*}+\alpha$ (spectator)
$\rightarrow {}^{162}Ho+\alpha$ (spectator) $+ pxn \quad (x=3)$,
(iii) $^{16}O(^{12}C+\alpha)+{}^{154}Sm \rightarrow {}^{12}C+{}^{154}Sm$
$\rightarrow {}^{166}Er^{*}+\alpha$ (spectator)
$\rightarrow {}^{161}Ho+\alpha$ (spectator) $+ pxn \quad (x=4)$,
(iv) $^{16}O(^{12}C+\alpha)+{}^{154}Sm \rightarrow {}^{12}C+{}^{154}Sm$
$\rightarrow {}^{166}Er^{*}+\alpha$ (spectator)
$\rightarrow {}^{164}Dy+\alpha$ (spectator) $+ 2pxn \quad (x=0)$,
(v) $^{16}O(^{8}Be+{}^{8}Be)+{}^{154}Sm \rightarrow {}^{8}Be+{}^{154}Sm$
$\rightarrow {}^{162}Dy^{*}+2\alpha$ (spectator)
$\rightarrow {}^{160}Dy+2\alpha$ (spectator) $+ xn \quad (x=2)$.

These reaction channels indicate the occurrence of incomplete fusion involving the breakup of ^{16}O into $^{4}He + {}^{12}C$ and/or $^{8}Be + {}^{8}Be$ followed by the fusion of one of the fragments with target nucleus ^{154}Sm. The measured normalized yields $({}^{\text{Meas}}_{\text{Norm}}Y)$ of five ERs, $^{163-161}Ho$, ^{164}Dy, and ^{160}Dy, populated through ICF reaction channels respectively have been observed in coincidence with fast α and 2α particles emitted in the forward cone and are shown in Fig. 5(b). The normalized production yields for ERs $^{163-161}Ho$ and ^{164}Dy populated through α-emitting channels (identified from particle-forward gated spectra) are found to be constant up to spin $_{\text{Mean}}J \approx 11\hbar$, while the ERs ^{160}Dy populated through 2α-emitting channels (identified from α-forward gated spectra) are constant up to spin $_{\text{Mean}}J \approx 13\hbar$ respectively. The normalized yield becomes nearly constant towards the lower spin states, indicating the absence of feeding towards the lower members of yrast line transitions. Figure 5(b) also shows that the characteristic of the measured spin distributions of ERs $^{163-161}Ho$ and ^{164}Dy populated through fast α emitting channels (identified from particle–forward gated spectra) is similar as that observed for ER ^{160}Dy populated through fast 2α emitting channels (identified from α-forward gated spectra). It has also been observed from the figure that the spin $(_{\text{Mean}}J)$ at half yield, i.e., the mean input angular momentum for the ERs $^{163-161}Ho$, ^{164}Dy, and ^{60}Dy, are found to be $\approx 11\hbar$ and $13\hbar$ for α- and 2α-emitting channels (ICF reaction channels) respectively. It is clear from the present results of spin distributions that the production of fast α particle(s) takes place at a relatively higher input angular momentum than that of CF channels and supports the fact that ICF predominantly occurs due to the higher value of input angular momentum, in turn correlated to the higher value of impact parameters. In this condition, ICF leads to peripheral interaction. It is also observed from the present measured values of $_{\text{Mean}}J$ that the multiplicity of fast α particles increases with the driving input angular momentum, which further shows the variation of ℓ bins with different values of impact parameters at a given projectile energy. Moreover, it may also be inferred that no significant contribution is present for lower ℓ values in ICF. The values of critical angular momenta for the evaporation residues populated through CF, ICF-α, and ICF-2α emitting channels in the present studied system have also been calculated using the prescription given by Wilczynski *et al.* [37,53] for the fusion of ^{16}O, ^{12}C, and ^{8}Be with ^{154}Sm. The calculated critical angular momentum (ℓ_{crit}) values for the evaporation residues populated through CF, ICF-α, and ICF-2α emitting channels are found to be $45\hbar$, $37\hbar$, and $28\hbar$ respectively. As per the formalism of the sum-rule model, the ℓ_{crit} values for ICF-α and ICF-2α emitting channels would translate into limiting angular momentum values of $50\hbar$ and $56\hbar$ respectively in the entrance channel, which are close to the value of the maximum angular momentum of $54\hbar$. Thus, experimental values of driving input angular momenta for different channels should, in principle, be close to the ℓ_{crit} values given by the sum-rule model. However, experimental values are substantially lower compared to the respective calculated values of ℓ_{crit}. The difference between the values of entrance channel angular momenta for evaporation residues populated through the reaction channels CF, ICF-α, and ICF-2α indicates that there would be branching to different rotational bands for higher angular momentum values. This branching would combine into a ground state rotational band at lower ℓ values. Therefore, the actual ℓ distribution will be strongly modified by a side feeding pattern. The deviation between calculated and experimental values would increase with increasing population of lower ℓ waves as observed in the case of complete fusion. However, in the case of ICF channels, the collisions are expected to become more and more peripheral with decreasing mass transfer thereby minimizing the contribution from lower ℓ waves. Thus, deviation is the minimum in the case of the 2α channel which is expected to be most peripheral. Thus, the experimental values of the driving input angular momenta, though they cannot be compared with the calculated values on the absolute scale, can be used for comparison on a relative scale for different transfer channels.

The following approximate relation has been obtained in terms of driving mean input angular momentum for CF process and ICF process with different α multiplicity:

$$\ell^{\text{ICF\_}2\alpha xn} \approx 1.2\ell^{\text{ICF\_}\alpha pxn} \approx 1.6\ell^{\text{CF\_}xn/pxn/2pxn}. \qquad (4.1)$$

This observation indicates that the larger mass transfer channel is localized in the lower impact parameter range (having a larger overlap of the projectile and the target nuclei) and thus lower angular momentum range [54]. In fact the actual difference in the entrance angular momentum values will be larger because smaller mass transfer brings in smaller angular momentum.

The reliability and accuracy of measured relative yields against the spins of energy levels of various evaporation residues populated through CF and ICF dynamics has been checked using the same procedure as adopted in Refs. [43–45]. The experimentally measured relative yield of the individual evaporation residue has been extrapolated to $J = 0\hbar$, and the yield value at $J = 0\hbar (Y_{J=0})$ has been normalized with the total yield (the sum of all fusion-evaporation channels) to estimate the relative yield value of each evaporation residue. The same procedure has been followed for the relative production yield of individual evaporation residue, which was calculated using statistical model code PACE4 for normalization with

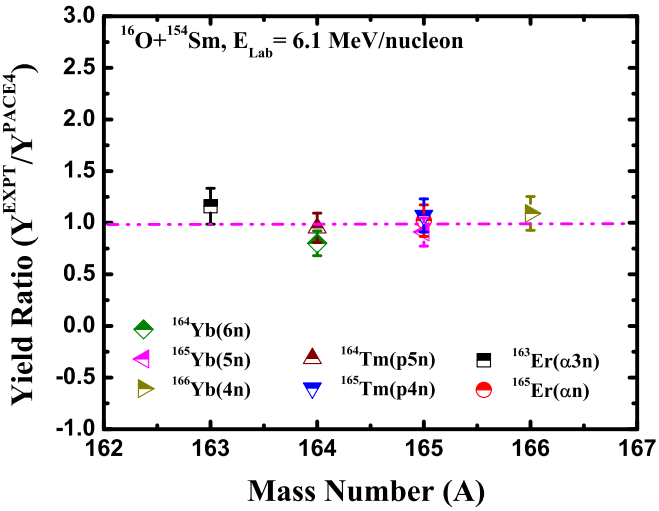

FIG. 6. The ratio of experimentally measured and theoretically calculated relative yields ($Y^{\mathrm{EXPT}}/Y^{\mathrm{PACE4}}$) for all fusion-evaporation channels. The experiment data for the evaporation residues ^{166}Yb($4n$), ^{165}Yb($5n$), ^{165}Tm($p4n$), ^{164}Tm($p5n$), ^{165}Er(αn), and ^{163}Er($\alpha 3n$) populated through CF has been taken from Ref. [48].

the total yield of fusion-evaporation channels. The ratio of experimentally measured and theoretically calculated relative yields ($Y^{\mathrm{EXPT}}/Y^{\mathrm{PACE4}}$) for all fusion-evaporation channels has been plotted in Fig. 6.

In order to get the clear picture of the feeding intensities in CF and ICF dynamics, an attempt has been made to estimate the feeding of intensities of ERs populated through CF and ICF from measured spin distributions. The measured feeding intensities of ERs populated through CF and ICF have been plotted as a function of observed spin $_{\mathrm{Obsd}}J$ in Figs. 7(a) and 7(b) respectively. As can be seen from Fig. 7(a), the feeding intensity in the CF process decreases exponentially toward higher spin states, which indicates a regular population with a strong feeding contribution for each γ-transition towards a lower spin state. This confirms the fact that the band is fed over a broad spin range in the CF reaction. However, as seen from Fig. 7(b), the feeding intensity of $^{163-161}$Ho (αpxn), ^{164}Dy ($\alpha 2pxn$), and ^{160}Dy ($2\alpha xn$) populated through ICF reaction channels (identified from forward gated spectra) are found to increase with decreasing $_{\mathrm{Obsd}}J$ up to $_{\mathrm{Mean}}J \approx 10\hbar$ and, $\approx 12\hbar$ values, respectively and then decreases towards the lower spin states, indicating its localization to a narrow angular momentum window. This may be attributable to less feeding probability in the ICF process caused by deexcitation of the evaporation residues.

A comparison of the average mean driving input angular momenta $\langle \ell \rangle$ of the ERs ^{164}Yb, ^{163}Tm, and ^{168,167}Er populated through the CF reaction and ERs ^{163,162,161}Ho and ^{164,160}Dy populated through the ICF reaction (α- and 2α-emitting channels) along with the CF, ICF-α, and ICF-2α reaction modes for the $^{16}\mathrm{O} + {}^{154}\mathrm{Sm}$ system at projectile energy 97.5 MeV has been done and is shown in Figs. 8(a) and 8(b). As can be seen from Fig. 8(a), the average value of mean input angular momenta $\langle \ell \rangle$ of ERs ^{163,162,161}Ho and ^{164,160}Dy

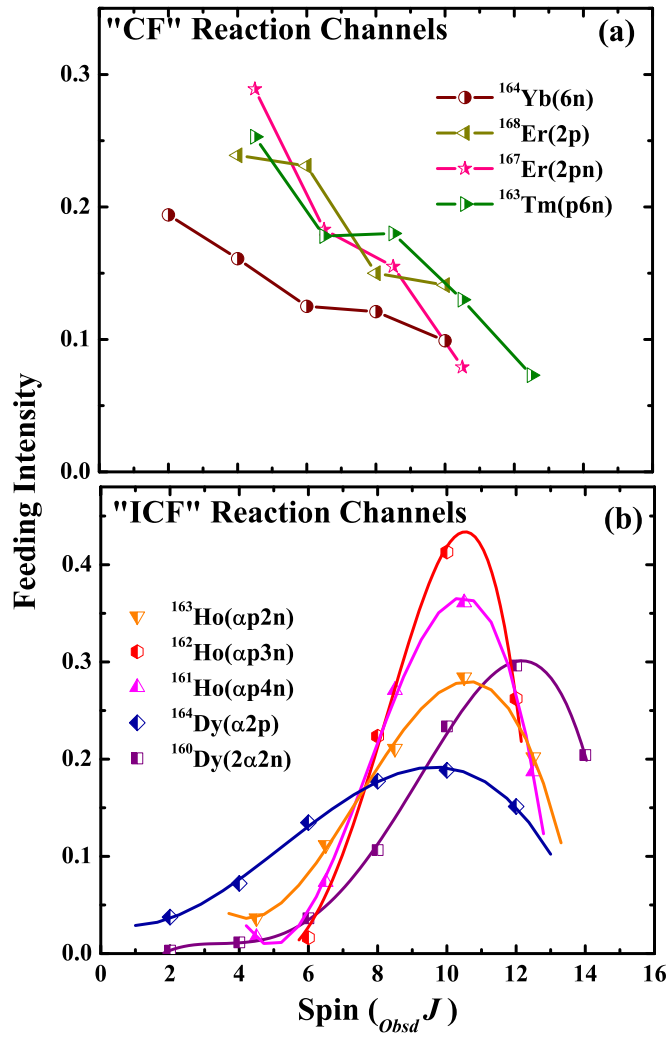

FIG. 7. Feeding intensity pattern of evaporation residues. (a) ^{164}Yb, ^{163}Tm, and ^{168,167}Er populated through CF reactions and (b) ^{163,162,161}Ho and ^{164,160}Dy populated through ICF reactions.

populated through ICF (α and 2α-emitting channels) reactions is enhanced $\approx$33% and $\approx$55% respectively from the ERs ^{164}Yb, ^{163}Tm, and ^{168,167}Er populated through CF. But $\langle \ell \rangle$ of ER ^{160}Dy populated through ICF (2α-emitting channels) reactions are enhanced $\approx$16% more than that of ^{163,162,161}Ho and ^{164}Dy populated through the ICF (α-emitting channels) reaction. Further, the comparison of the average mean driving input angular momenta $\langle \ell \rangle$ of ERs populated through CF and ICF reactions as a function of reaction modes for the same system and the same energy has been done and is also shown in Fig. 8(b). It has been observed from this figure that the $\langle \ell \rangle$ of ERs populated through the ICF reaction is enhanced $\approx$44% from the $\langle \ell \rangle$ of ERs populated through CF channels. The above comparison shows that the population of high spin states through 2α-emitting channels (ICF reaction channels) is larger than that of α-emitting channels (ICF reaction channels) and CF reactions. The present observations also indicate a larger population of high spin states through the ICF process.

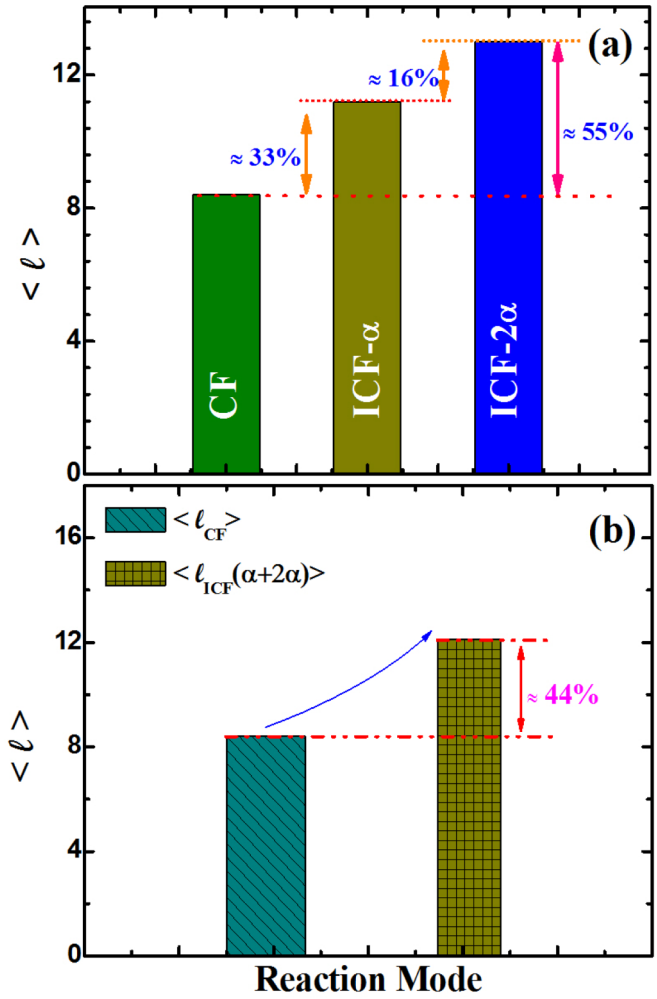

FIG. 8. The average value of mean input angular momenta $\langle \ell \rangle$ of evaporation residues produced through (a) CF, ICF-α, and ICF-2α emission and (b) CF and ICF reactions ($\alpha + 2\alpha$ channels) as a function of different observed reaction modes in the $^{16}O + ^{154}Sm$ system at projectile energy 97.5 MeV.

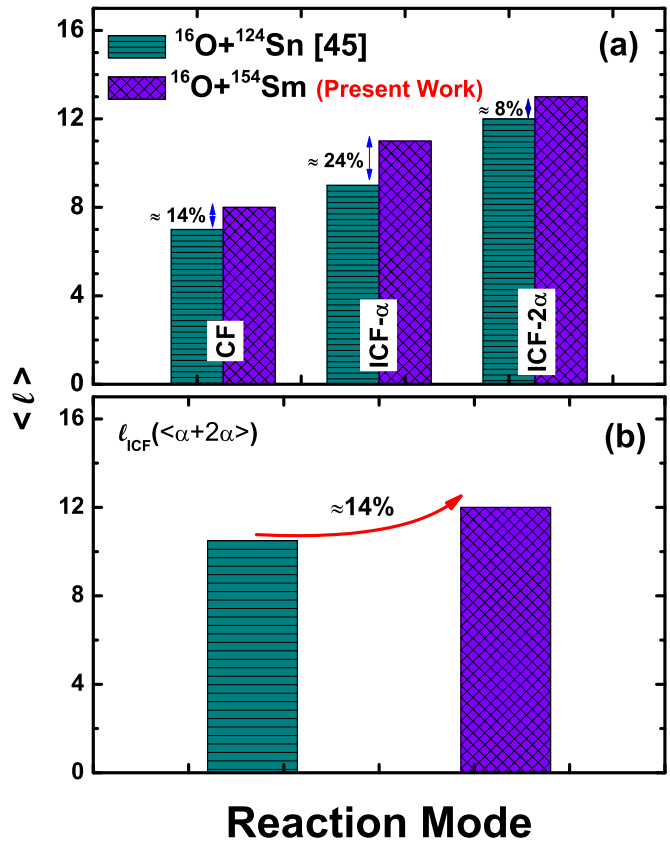

FIG. 9. (a) The mean value of input angular momenta involved in various CF and ICF (α- and 2α-emitting channels) reactions and (b) a comparison of average mean value $\langle \ell \rangle$ of input angular momenta involved in ICF ($\alpha + 2\alpha$ channels) as a function of ICF reaction modes for the $^{16}O + ^{124}Sn$ [45] and $^{16}O + ^{154}Sm$ systems at projectile energy 97.5 MeV.

V. DEPENDENCE OF ICF DYNAMICS ON TARGET DEFORMATION AND MASS ASYMMETRY

A comparison of the mean input angular momentum for the ICF channels populated in $^{16}O + ^{124}Sn$ (spherical) [45] and $^{16}O + ^{154}Sm$ (deformed) systems with same projectile and energy has been done in Figs. 9(a) and 9(b). Figure 9(a) shows that the mean input angular momentum for CF and ICF (α- and 2α-emitting channels) reactions are found to be ${}_{\text{Mean}}J \approx 7\hbar, \approx 9\hbar$, and $\approx 12\hbar$ respectively for the $^{16}O + ^{124}Sn$ (spherical) system, while in the case of the present system $^{16}O + ^{154}Sm$ (deformed), the mean input angular momentum for CF and ICF (α- and 2α-emitting channels) reactions are found to be ${}_{\text{Mean}}J \approx 8\hbar, \approx 11\hbar$, and $\approx 13\hbar$ respectively. From Fig. 9(a), the value of mean input angular momentum of ERs populated through CF channels in the $^{16}O + ^{154}Sm$ system is higher, $\approx$14%, than that of mean input angular momentum value of ERs populated through CF channels in $^{16}O + ^{124}Sn$ systems. It is also clear from this figure that the mean input angular momentum values of ERs populated through ICF reactions (α- and 2α-emitting channels) in the $^{16}O + ^{154}Sm$ system is relatively higher, $\approx$24% and $\approx$8%, than that of mean input angular momentum values of ERs populated through ICF reactions (α- and 2α-emitting channels) in the $^{16}O + ^{124}Sn$ system respectively. The present comparison of mean input angular momentum values indicates that the ERs produced through CF and ICF reaction channels populate with a higher value of spin states in a deformed target than that of a spherical target. Further, a comparison of average mean $\langle \ell \rangle$ value of ERs populated through ICF (α- and 2α-emitting channels) reactions for a similar value of maximum angular momentum (ℓ_{Maxm}) for the two systems $^{16}O + ^{124}Sn$ and $^{16}O + ^{154}Sm$ has been done and is shown in Fig. 9(b). These systems $^{16}O + ^{124}Sn$ and $^{16}O + ^{154}Sm$ have ℓ_{Maxm} values $\approx 56\hbar$ and $\approx 54\hbar$ respectively at the same projectile and energy. The value of ℓ_{Maxm} has been calculated using the expression given in Ref. [37]. It has been noticed from Fig. 9 (b) that the average mean $\langle \ell \rangle$ value of ERs populated through ICF (both $\alpha + 2\alpha$-emitting channels) reactions in the $^{16}O + ^{154}Sm$ system is found to be $\approx$14% higher than that of the average mean $\langle \ell \rangle$ value of ERs populated through ICF (both $\alpha + 2\alpha$ emitting channels) reactions in the $^{16}O + ^{124}Sn$ system. These results confirm the fact that the ICF

reactions not only depend on the mass asymmetry between the projectile target systems, but also depend on deformation of the target.

VI. SUMMARY AND CONCLUSIONS

Spin distributions of ERs populated through CF and ICF have been measured for the $^{16}O + ^{154}Sm$ system at energy 97.5 MeV. The charged-particle ($Z = 1,2$)–γ-ray coincidence technique has been used for obtaining the spin distributions of ERs populated through CF and/or ICF reactions in the present work. The results indicate the occurrence of incomplete-fusion involving the breakup of ^{16}O into $^{4}He + ^{12}C$ and/or $^{8}Be + ^{8}Be$ followed by fusion of one of the fragments with target (^{154}Sm) nucleus. The spin distributions are found to be distinct for ICF channels from that of CF channels. The feeding intensity profile of ERs populated through CF and ICF dynamics has also been investigated using spin distributions of ERs. In ICF channels, the population of low spin states are observed to be very strongly hindered and/or less fed, while in the case of CF significant feeding of γ transitions has been observed over a broad spin range. In the present study, the mean input angular momentum for ICF channels is found to be significantly higher compared to CF channels. The present observation clearly shows that the incomplete fusion occurs due to production of fast α particles, which are forward peaked, arising from the relatively larger input angular momentum in the entrance channel and hence arising from noncentral collisions. The comparison of mean input angular momenta values of CF and ICF (α- and 2α-emitting channels) reactions show that the population of high spin states through only ICF (2α-emitting channels) is larger than that of ICF (α-emitting channels) and CF reactions. The present results clearly indicate that the population of high spin states takes place through the ICF process. In addition, comparison of present results with earlier measurements indicates that the ERs produced through CF and ICF reaction channels populate with a higher value of spin states in a deformed target than that of a spherical target. The value of mean input angular momenta for ICF shows an enhancement with target deformation indicating involvement of more peripheral collisions in deformed targets. The present results also show that the ICF reactions not only depend on the mass asymmetry between the projectile target systems, but also depend on deformation of the target.

ACKNOWLEDGMENTS

The authors are thankful to the Director, Inter University Accelerator Center (IUAC), New Delhi, India for providing the experimental facilities for carrying out this work. The authors are thankful to Mr. S. R. Abhilash, Target Lab, and operational staff of Pelletron Accelerator, IUAC, New Delhi, for providing good cooperation during the course of this experiment. The authors are also thankful to Dr. R. K. Bhowmik, IUAC, New Delhi for suggesting this type of experiment for the study of ICF dynamics. D.S. acknowledges encouragement from the Vice Chancellor of Central University of Jharkhand (CUJ), Ranchi, India. The authors express their thanks to the Head, Centre for Applied Physics, CUJ, Ranchi, for providing the necessary facilities during the present work. D.S. is also thankful to the Department of Science and Technology (DST), New Delhi, India for providing financial support through SERC-Fast Track Scheme for Young Scientist (Grant No. SR/FTP/PS-005/2011), University Grant Commission (UGC), New Delhi, India through UGC-BSR startup grant [Grant No. F.30-14/2014(BSR)] and IUAC, New Delhi research project (Ref. IUAC/XIII.3A/UFR/54321) respectively. One of the authors, S.B.L., acknowledges University Grant Commission (UGC) of the Government of India for providing financial support in the form of a Rajiv Gandhi National Fellowship for ST students (Reg. No. RGNF-2014-15-ST-JHA-60266). Authors are thankful to Dr. B. S. Tomar, BARC, Mumbai for scientific discussion to improve this paper.

[1] P. Vergani, E. Gadioli, E. Vaciago, E. Fabrici, E. Gadioli Erba, M. Galmarini, G. Ciavola, and C. Marchetta, Phys. Rev. C **48**, 1815 (1993).
[2] M. Dasgupta, P. R. S. Gomes, D. J. Hinde, S. B. Moraes, R. M. Anjos, A. C. Berriman, R. D. Butt, N. Carlin, J. Lubian, C. R. Morton, J. O. Newton, and A. Szanto de Toledo, Phys. Rev. C **70**, 024606 (2004).
[3] M. Cavinato, E. Fabrici, E. Gadioli, E. Gadioli Erba, P. Vergani, M. Crippa, G. Colombo, I. Redaelli, and M. Ripamonti, Phys. Rev. C **52**, 2577 (1995).
[4] E. Gadioli, C. Birattari, M. Cavinato, E. Fabrici, E. Gadioli Erba, V. Allori, E. Cerutti, A. Di Filippo, S. Vailati, T. G. Stevens, S. H. Connell, L. E. E. Sellschop, E. M. Nortier, G. E. Steyn, and C. Marchetta, Nucl. Phys. A **641**, 271 (1998).
[5] P. R. S. Gomes, I. Padrona, M. D. Rodríguez, G. V. Martí, R. M. Anjos, J. Lubian, R. Veiga, R. Liguori Neto, E. Crema, N. Added, L. C. Chamon, J. O. Fernández Niello, O. A. Capurro, A. J. Pacheco, J. E. Testoni, D. Abriola, A. Arazi, M. Ramírez, and M. S. Hussein, Phys. Lett. B **601**, 20 (2004).
[6] M. Dasgupta, D. J. Hinde, A. Mukherjee, and J. O. Newton, Nucl. Phys. A **787**, 144 (2007).
[7] A. Diaz-Torres, D. J. Hinde, J. A. Tostevin, M. Dasgupta, and L. R. Gasques, Phys. Rev. Lett. **98**, 152701 (2007).
[8] D. J. Parker, J. Asher, T. W. Conlon, and I. Naqib, Phys. Rev. C **30**, 143 (1984)
[9] M. Crippa, E. Gadioli, P. Vergani, G. Ciavola, C. Marchetta, and M. Bonardi, Z. Phys. A: Hadrons Nucl. **350**, 121 (1994).
[10] H. C. Britt and A. R. Quinton, Phys. Rev. **124**, 877 (1961).
[11] J. Galin, B. Gatty, D. Guerreau, C. Rousset, U. C. Schlotthauer-Voos, and X. Tarrago, Phys. Rev. C **9**, 1126 (1974).
[12] T. Inamura, M. Ishihara, T. Fukuda, T. Shimoda, and H. Hirutal, Phys. Lett. B **68**, 51 (1977).
[13] D. J. Parker, J. J. Hogan, and J. Asher, Phys. Rev. C **39**, 2256 (1989).
[14] B. S. Tomar, A. Goswami, A. U. R. Reddy, S. K. Das, P. P. Burte, S. B. Manohar, and B. John, Phys. Rev. C **49**, 941 (1994).
[15] B. S. Tomar, A. Goswami, A. U. R. Reddy, S. K. Das, P. P. Burte, S. B. Manohar, and B. John, Nucl. Phys. A **776**, 83 (2006).

[16] M. K. Sharma, U. Gupta, B. K. Sharma, B. P. Singh, H. D. Bhardwaj, R. Kumar, K. S. Golda, and R. Prasad, Phys. Rev. C **70**, 044606 (2004).

[17] D. Singh, M. A. Ansari, R. Ali, N. P. M. Sathik, and M. Ismail, J. Phys. Soc. Jpn. **75**, 104201 (2006).

[18] H. Morgenstern, W. Bohne, W. Galster, and K. Grabisch, Phys. Rev. Lett. **52**, 1104 (1984).

[19] D. Singh, R. Ali, M. A. Ansari, M. H. Rashid, R. Guin, and S. K. Das, Nucl. Phys. A **879**, 107 (2012).

[20] R. Ali, D. Singh, M. A. Ansari, M. H. Rashid, R. Guin, and S. K. Das, J. Phys. G: Nucl. Part. Phys. **37**, 115101 (2010).

[21] H. Kumar, S. A. Tali, M. A. Ansari, D. Singh, R. Ali, K. Kumar, N. P. M. Sathik, S. Parashari, A. Ali, and R. Dubey, Nucl. Phys. A **960**, 53 (2017).

[22] S. Chakrabarty, B. S. Tomar, A. Goswami, G. K. Gubbi, S. B. Manohar, A. Sharma, B. B. Kumar, and S. Mukherjee, Nucl. Phys. A **678**, 355 (2000).

[23] A. Gavron, Phys. Rev. C **21**, 230 (1980).

[24] L. Westerberg, D. G. Sarantites, D. C. Hensley, R. A. Dayras, M. L. Halbert, and J. H. Barker, Phys. Rev. C **18**, 796 (1978).

[25] K. A. Geoffroy, D. G. Sarantites, M. L. Halbert, D. C. Hensley, R. A. Dayras, and J. H. Barker, Phys. Rev. Lett. **43**, 1303 (1979).

[26] K. Siwek-Wilczynska, E. H. du Marchie van Voorthuysen, J. van Popta, R. H. Siemssen, and J. Wilczynski, Nucl. Phys. A **330**, 150 (1979); K. Siwek-Wilczyński, E. H. duMarchie van Voorthuysen, J. Van Popta, R. H. Siemssen, and J. Wilczyński, Phys. Rev. Lett. **42**, 1599 (1979).

[27] H. Yamada, C. F. Maguire, J. H. Hamilton, A. V. Ramayya, D. C. Hensley, M. L. Halbert, R. L. Robinson, F. E. Bertrand, and R. Woodward, Phys. Rev. C **24**, 2565 (1981).

[28] D. R. Zolnowski, H. Yamada, S. E. Cala, A. C. Kahler, and T. T. Sugihara, Phys. Rev. Lett. **41**, 92 (1978).

[29] J. H. Barker, J. R. Beene, M. L. Halbert, D. C. Hensley, M. Jääskeläinen, D. G. Sarantites, and R. Woodward, Phys. Rev. Lett. **45**, 424 (1980).

[30] T. Inamura, A. C. Kahler, D. R. Zolnowski, U. Garg, T. T. Sugihara, and M. Wakai, Phys. Rev. C **32**, 1539 (1985).

[31] D. Hojman, M. A. Cardona, A. Arazi, O. A. Capurro, J. O. Fernández-Niello, G. V. Martí, A. J. Pacheco, J. E. Testoni, D. Bazzacco, A. Burlon, J. Davidson, M. Davidson, G. de Angelis, M. De Poli, M. E. Debray, A. Gadea, A. J. Kreiner, S. M. Lenzi, S. Lunardi, N. H. Medina, D. R. Napoli, C. Rossi Alvarez, and C. Ur, Phys. Rev. C **73**, 044604 (2006).

[32] T. Inamura, T. Kojima, T. Nomura, T. Sugitate, and H. Utsunomiya, Phys. Lett. B **84**, 71 (1982).

[33] W.Trautmann, Ole Hansen, H. Tricoire, W. Hering, R. Ritzka, and W. Trombik, Phys. Rev. Lett. **53**, 1630 (1984).

[34] C. Gerschel, Nucl. Phys. A **387**, 297 (1982).

[35] I. Tserruya, V. Steiner, Z. Fraenkel, P. Jacobs, D. G. Kovar, W. Henning, M. F. Vineyard, and B. G. Glagola, Phys. Rev. Lett. **60**, 14 (1988).

[36] T. Udagawa and T. Tamura, Phys. Rev. Lett. **45**, 1311 (1980).

[37] J. Wilczynski, K. Siwek-Wilczynska, J. Van Driel, S. Gonggrijp, D. C. J. M. Hageman, R. V. F. Janssens, J. Lukasiak, R. H. Siemssen, and S. Y. Van der Werf, Nucl. Phys. A **373**, 109 (1982).

[38] M. C. Mermaz, R. Dayras, J. Barrette, B. Berthier, D. M. De Castro Rizzo, O. Cisse, R. Legrain, A. Pagano, E. Pollacco, H. Delagrange, W. Mittig, B. Heusch, G. Lanzano, and A. Palmeri, Nucl. Phys. A **441**, 129 (1985).

[39] J. P. Bondorf, J. N. De, G. Fái, A. O. T. Karvinen, B. Jakobsson, and J. Randrup, Nucl. Phys. A **333**, 285 (1980).

[40] R. Weiner and M. Westrom, Nucl. Phys. A **286**, 282 (1977).

[41] D. H. E. Gross and J. Wilczynski, Phys. Lett. B **67**, 1 (1977).

[42] G. D. Dracoulis, A. P. Byrne, T. Kibédi, T. R. McGoram, and S. M. Mullins, J. Phys. G: Nucl. Part. Phys. **23**, 1191 (1997).

[43] P. P. Singh, B. P. Singh, M. K. Sharma, Unnati. R. Kumar, K. S. Golda, D. Singh, R. P. Singh, S. Muralithar, M. A. Ansari, R. Prasad, and R. K. Bhowmik, Phys. Rev. C **78**, 017602 (2008).

[44] P. P. Singh, B. P. Singh, M. K. Sharma, U. Gupta, R. Kumar, D. Singh, R. P. Singh, S. Murlithar, M. A. Ansari, R. Prasad, and R. K. Bhowmik, Phys. Lett. B **671**, 20 (2009).

[45] D. Singh, R. Ali, M. A. Ansari, K. S. Babu, P. P. Singh, M. K. Sharma, B. P. Singh, R. K. Sinha, R. Kumar, S. Muralithar, R. P. Singh, and R. K. Bhowmik, Phys. Rev. C **81**, 027602 (2010).

[46] V. R. Sharma, Pushpendra P. Singh, M. Shuaib, A. Yadav, I. Bala, M. K. Sharma, S. Gupta, D. P. Singh, R. Kumar, S. Muralithar, R. P. Singh, B. P. Singh, R. Prasad, and R. K. Bhowmik, J. Phys. G: Nucl. Part. Phys. **42**, 055113 (2015).

[47] V. R. Sharma, P. P. Singh, Mohd. Shuaib, A. Yadav, I. Bala, M. K. Sharma, S. Gupta, D. P. Singh, R. Kumar, S. Muralithar, R. P. Singh, B. P. Singh, R. Prasad, and R. K. Bhowmik, Nucl. Phys. A **946**, 182 (2016).

[48] D. Singh, S. B. Linda, P. K. Giri, A. Mahato, R. Tripathi, H. Kumar, M. Afzal Ansari, N. P. M. Sathik, R. Ali, R. Kumar, S. Muralithar, and R. P. Singh, Phys. Lett. B **774**, 7 (2017).

[49] The Stopping and Range of Ions in Matter (SRIM-2008.04); http://www.srim.org/.

[50] CANDLE, Data acquisition and analysis software, designed to support the accelerator based experiments at the Inter-University Accelerator Centre IUAC), New Delhi, India; http://www.iuac.res.in/NIAS/.

[51] S. Muralithar, B. Mukherjee, R. P. Singh, G. Mukherjee, P. Joshi, A. Punithan, B. K. Sahu, A. Gupta, R. Ahuja, R. Ram, S. Rao, S. K. Saini, J. Zacharis, and R. K. Bhowmik, Nucl. Instrum. Methods Phys. Res. A **729**, 849 (2013).

[52] RADWARE, the level scheme directory on http://radware.phy.ornl.gov/agsdir1.html.

[53] J. Wilczynski, K. Siwek-Wilczynska, J. van Driel, S. Gonggrijp, D. C. J. M. Hageman, and R. V. F. Janssens, Phys. Rev. Lett. **45**, 606 (1980).

[54] R. Tripathi, K. Sudarshan, S. Sodaye, A. V. R. Reddy, A. Goswami, B. K. Nayak, and S. K. Sharma, Phys. Rev. C **79**, 064604 (2009).